Journal of Colloid and Interface Science 512 (2018) 767–774

Contents lists available at ScienceDirect

Journal of Colloid and Interface Science

journal homepage: www.elsevier.com/locate/jcis

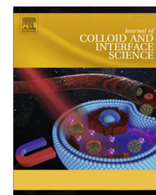

Regular Article

Digital to analog resistive switching transition induced by graphene buffer layer in strontium titanate based devices

Tao Wan [a], Bo Qu [a], Haiwei Du [a], Xi Lin [a], Qianru Lin [a], Da-Wei Wang [b], Claudio Cazorla [a,*], Sean Li [a], Sidong Liu [c,*], Dewei Chu [a,*]

[a] School of Materials Science and Engineering, The University of New South Wales, Sydney 2052, Australia
[b] School of Chemical Engineering, The University of New South Wales, Australia
[c] Sydney Medical School, The University of Sydney, Australia

GRAPHICAL ABSTRACT

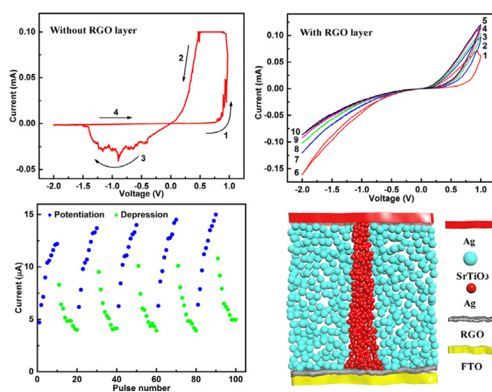

ARTICLE INFO

Article history:
Received 21 August 2017
Revised 27 October 2017
Accepted 31 October 2017
Available online 31 October 2017

Keywords:
Digital resistive switching
Analog resistive switching
Reduced graphene oxide
$SrTiO_3$

ABSTRACT

Resistive switching behaviour can be classified into digital and analog switching based on its abrupt and gradual resistance change characteristics. Realizing the transition from digital to analog switching in the same device is essential for understanding and controlling the performance of the devices with various switching mechanisms. Here, we investigate the resistive switching in a device made with strontium titanate ($SrTiO_3$) nanoparticles using X-ray diffractometry, scanning electron microscopy, Raman spectroscopy, and direct electrical measurements. It is found that the well-known rupture/formation of Ag filaments is responsible for the digital switching in the device with Ag as the top electrode. To modulate the switching performance, we insert a reduced graphene oxide layer between $SrTiO_3$ and the bottom FTO electrode owing to its good barrier property for the diffusion of Ag ions and high out-of-plane resistance. In this case, resistive switching is changed from digital to analog as determined by the modulation of interfacial resistance under applied voltage. Based on that controllable resistance, potentiation and depression behaviours are implemented as well. This study opens up new ways for the design of multifunctional devices which are promising for memory and neuromorphic computing applications.

© 2017 Published by Elsevier Inc.

* Corresponding authors.
E-mail addresses: c.cazorla@unsw.edu.au (C. Cazorla), sidong.liu@sydney.edu.au (S. Liu), d.chu@unsw.edu.au (D. Chu).

https://doi.org/10.1016/j.jcis.2017.10.113
0021-9797/© 2017 Published by Elsevier Inc.

1. Introduction

Memristors with metal-insulator-metal (MIM) sandwich structures have been widely investigated because of their potential applications in non-volatile memory (NVM), logic operations and neuromorphic computing [1,2]. Resistive switching properties in memristors are closely associated with the change of internal states under external stimuli, such as light, magnetic and electric field. In general, the switching behaviours can be classified into two modes: digital and analog switching [3].

Abrupt change of resistance in digital switching gives rise to the distinguished states, which are beneficial for the information storage. This is ascribed to the formation and rupture of highly conductive filaments between the electrodes caused by migration of oxygen vacancies or active metal ions (Ag^{+}, Cu^{2+}, Ni^{3+}, Al^{3+}, In^{3+}, etc.). Based on a series of characterizations, the evolutions of active metals, oxygen vacancies or oxygen-deficient filaments, have been observed during their switching processes respectively [4–8]. The simultaneous observation of dual-filament consisting of oxygen vacancies and Ag has been also reported very recently [9]. By controlling the filaments growth and dissolution, the low-resistance state (LRS or on state) and high-resistance state (HRS or off state) can be switched easily in the devices. Normally, on/off resistance ratio of more than 10 is needed to realize data storage and low misreading rate [10,11]. Moreover, a relatively high on/off ratio (above 10^6) has been reported in many studies, which provides a large memory operation window and facilitates practical memory applications [12,13]. Furthermore, multilevel resistive switching (MRS) devices with as many as 8 states have been fabricated, enabling high-density data storage [14,15].

In contrast to digital switching, analog switching exhibits a gradual change of resistance. This type of switching bears some similarities with the adaptive change of learning state in biological synapses, which are the basic building blocks of a brain and responsible for the learning and memory behaviours [16]. Therefore, a variety of memristors have been investigated to emulate the synaptic functions, including long-term/short-term plasticity (LTP and STP), and spike-time-dependent plasticity (STDP) [17]. These memristive devices acting as artificial synapses can contribute to the realization of artificial neural networks for significantly improving the efficiency of information processing tasks in conventional digital computers.

To better understand the switching mechanisms and improve the performance, many studies have been carried out to implement both digital and analog switching in a same device. By controlling the experimental conditions, the coexistence of both behaviours has been found in several devices, including Ag/$CH_3NH_3PbI_{3-x}Cl_x$/FTO [18], Pt/$BiFeO_3$/Pt [19] and Ag/MoO_{3-x}/FTO [20]. In addition, the transition from digital to analog switching can be induced by varying the electrodes and insulator thickness [21,22]. For digital switching, the random rupture/formation of the filaments usually leads to high variability and low reliability of the devices. An interesting approach to modulate the switching performance consists in deliberately inserting an additional layer in the metal-insulator-metal sandwich to improve the controllability of filaments formation and rupture. For example, the metal oxide layers, such as Al_2O_3 [23], TaO_x [24] and TiO_x [25], have been proposed to improve the switching performance.

Recently, graphene has also been widely employed in memristors as an excellent barrier layer to prevent the penetration of molecules, gases as well as metals (Al, Cu, Ag, etc.). After inserting the graphene, excessive injection of metal ions and filament overgrowth can be effectively suppressed, leading to enhanced performance (e.g., increased uniformity and reliability). By using nanopore graphene layer in the memory device, the filament formation was confined as well [26,27]. As its typical derivatives, graphene oxide (GO) and reduced graphene oxide (RGO) thin films similarly exhibit good barrier function as well [28,29]. Apart from facilitating uniform switching, reduced power consumption owing to the high out-of-plane resistance of graphene has been reported [10,30,31].

Here, the $SrTiO_3$ nanoparticles based memristors have been prepared by a facile solution-based method with using Ag and fluorine doped tin oxide (FTO) coated glass as top and bottom electrode respectively. The $SrTiO_3$ device without GO showed typical digital switching with a small on/off ratio, poor endurance and retention due to random formation/rupture Ag filament and porous structure of $SrTiO_3$ nanoparticles film. However, after inserting the reduced graphene oxide into the $SrTiO_3$/FTO interface, we found that low operational current can be achieved without setting compliance currents. Furthermore, the Ag/$SrTiO_3$/RGO/FTO device exhibited uniform analog switching with good performance; the corresponding synaptic behaviours, including potentiation/depression, were also investigated.

2. Experimental section

2.1. Material synthesis and device fabrication

$SrTiO_3$ nanoparticles were synthesized by a solution-based method at low temperature (80 °C) and were assembled into films by drop-coating based on the previous report [32]. FTO was used as bottom electrode and silver paste with diameter less than 400 μm was selected as top electrode. The final sample Ag/$SrTiO_3$/FTO was dried in oven at 150 °C for 1 h [33]. The Ag/$SrTiO_3$/RGO/FTO device was fabricated under same procedures except that RGO film was firstly formed on FTO glass. In detail, 20 μL of GO solution (1.15 mg/mL) prepared by Hummers method [34] was dropped onto the FTO substrate which was pre-cleaned with ethanol and deionized water, and further treated with ultraviolet radiation for 1 h. After the GO sample was dried, it was sintered in the furnace at 350 °C for 10 min in air to realize the moderate reduction as previously reported [35].

2.2. Characterization and electrical measurement

The crystalline phases of the samples were characterized by X-ray diffractometer with Cu Ka radiation (The PANalytical Xpert Multipurpose X-ray Diffraction System). The cross-section images of the sample were obtained with scanning electron microscopy (FE-SEM, FEI Nova Nano SEM 450). The Raman spectroscopy was measured by an inVia Renishaw Raman microscope excited by a 514 nm laser. The electrical measurements of the samples were carried out using a Keysight b2902a source meter at room temperature.

3. Results and discussion

Fig. 1(a–c) shows the switching characteristics of the Ag/$SrTiO_3$/FTO device with different compliance current (I_{cc}). Upon applying a voltage following the sequence $0\ V \rightarrow 1\ V \rightarrow 0\ V \rightarrow -2\ V \rightarrow 0\ V$, bipolar switching behaviours are observed. An abrupt change of resistance from HRS to LRS occurs when the positive voltage reaches about 1 V (SET process). We attribute the small set voltage to a large ion flux caused by the large diffusion coefficient of Ag^{+} ions, as it has been shown elsewhere [36,37]. Meanwhile, no forming process is required for the switching behaviours. Subsequent application of negative voltage switches the device back to the HRS (RESET process). Generally, for digital switching, appropriate

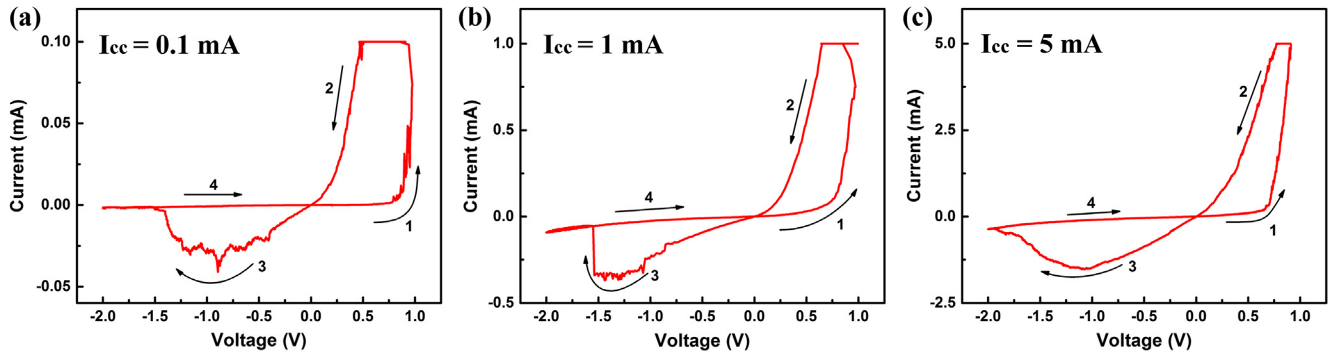

Fig. 1. I-V curves of Ag/$SrTiO_3$/FTO under different I_{cc}. (a) I_{cc} = 0.1 mA; (b) I_{cc} = 1 mA; (b) I_{cc} = 5 mA.

I_{cc} needs to be applied to avoid the breakdown of the device and tune the LRS state. Higher I_{cc} can be used to obtain a higher on/off ratio but the device lifetime then is also shortened. If the I_{cc} is too low, switching behaviour will not be stable as the weak filaments can be easily dissolved [38]. Here, we choose I_{cc} = 100 μA to limit the current and study the endurance and retention behaviours, as shown in Fig. 2(a, b). The resistance of LRS is kept stable during the tests due to the applied I_{cc}. A small on/off ratio of about 15 is achieved within the first 400 cycles, but the resistance of HRS decreases gradually with further increasing the switching cycles. In addition, a noticeable fluctuation of HRS is observed in the device after 200 s, exhibiting a low stability.

The switching behaviours Ag/$SrTiO_3$/FTO can be explained in terms of the formation and dissolution of Ag filaments. When a positive voltage is applied on the Ag top electrode, Ag is oxidized. The obtained Ag^+ ions migrate to the FTO bottom electrode and are reduced to Ag when in contact with FTO. Consequently, the conductive Ag filaments connecting the two electrodes lead to the transition from HRS to LRS. The device will be switched back to HRS by means of a voltage with the opposite polarity, resulting in the rupture of Ag filaments (Fig. 2(c, d)). The dynamic process of formation and dissolution of filaments has been observed by in situ TEM in other studies [9,39,40]. It was reported that different I_{cc} can modify the growth of Ag filaments, including their morphology, size and

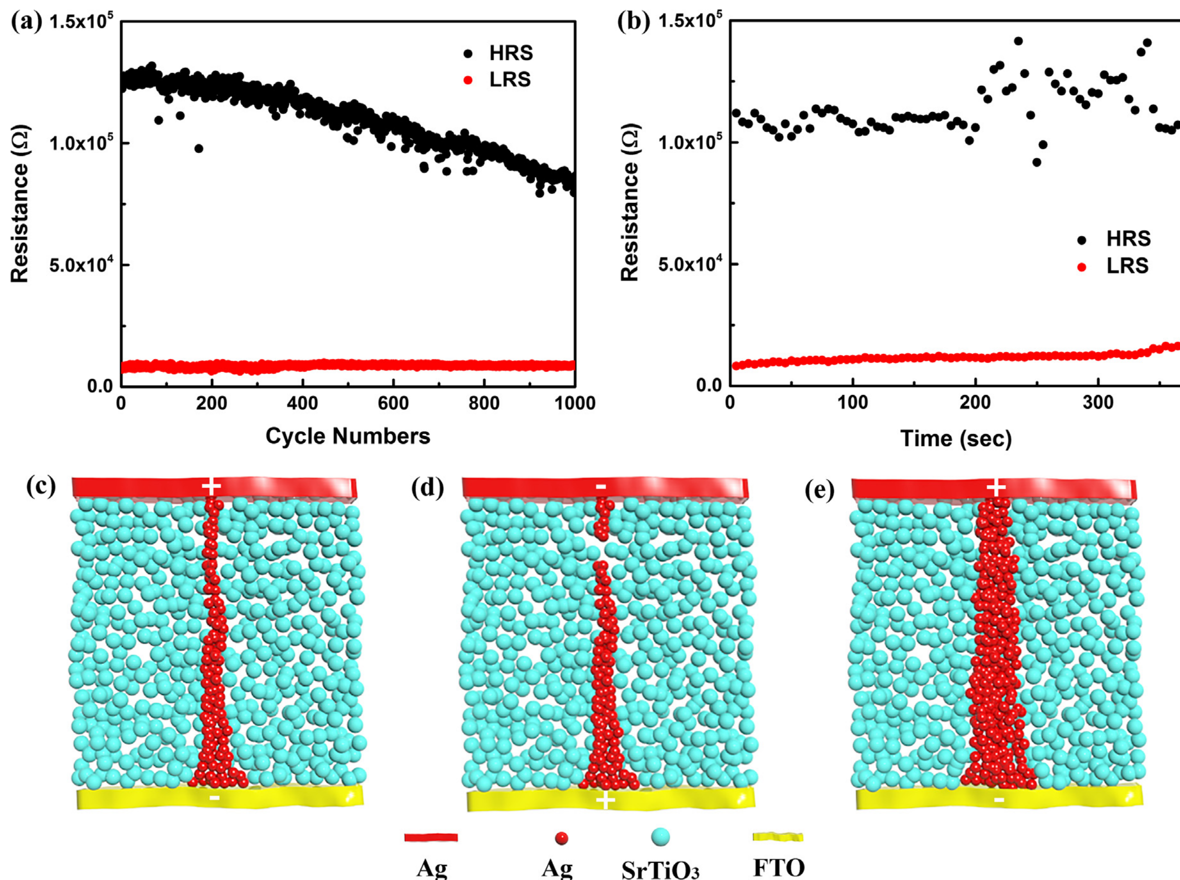

Fig. 2. (a) Endurance test of the Ag/$SrTiO_3$/FTO device with an I_{cc} of 0.1 mA. Set and reset pulses are +1.2 V and −2 V respectively with duration of 5 ms. (b) Retention test of the Ag/$SrTiO_3$/FTO at room temperature. Schematic illustrations of proposed switching mechanism: (c) set and (d) reset process with low I_{cc} (e.g. 0.1 mA). (e) Set process with high or no I_{cc}.

density, bringing about the controlled resistance of the device [38]. For the higher I_{cc}, e.g., 5 mA, a strong filament may be obtained as well as lower resistance (Fig. 2(e)). The high volume of the filament which is difficult to be ruptured, induces the gradual reset [41].

However, the filamentary switching suffers from high variability and low reliability due to random rupture/formation of the filaments. On the other hand, the existence of pores in the film facilitates the accumulation of Ag in the system, giving rise to greatly reduced initial resistance and hence to small on/off ratio. Furthermore, the slow growth of Ag filaments during repetitive pulse cycles is responsible for the gradual decrease of HRS resistance. Similar phenomena also have been reported in devices based on Cu and oxygen vacancy filaments [42,43].

To control the Ag filament growth and resistive switching behaviour, RGO film was introduced. As shown in Fig. 3(a), the solution processed GO exhibits a typical peak at $2\theta = 9.7°$, which belongs to the diffraction of the (0 0 2) plane. Apart from the peaks of crystalline phases of the used FTO substrate, only a weak and broad diffraction peak at about 25° is observed in the sample after the thermal treatment at 350 °C for 10 min, which indicates that the GO is reduced to RGO [35]. From the Raman spectra of GO and RGO (Fig. 3(b)), two peaks at about 1355 and 1600 cm^{-1} are observed, corresponding to the D and G band respectively. The D band is related to structural defects and partially disordered structures while the G band represents E_{2g} vibration mode of the sp^2 carbon [44]. Similar to other works, a slight increase of the relative intensity ratio of the D and G band (I_D/I_G) is seen in RGO. This is normally due to the increase of the number of graphene domains with smaller average size or higher defect density [45,46].

Interestingly, the digital switching behaviour changes to analog switching behaviour after inserting the RGO layer into the device, as shown in Fig. 4(a, b). We also investigated the endurance and retention properties in this case. The device exhibits a much smaller on/off ratio of ~1.5, which is about one-tenth of that without RGO layer. However, much better uniformity of switching behaviour is achieved, which could last for up to 1×10^4 cycles (Fig. 4(c)). The fluctuation observed in the device can be ascribed to a relatively small switching window. The stable retention characteristics of HRS and LRS for ~10^4 s are also observed (Fig. 4(d)).

Synaptic plasticity, which is in charge of memory and learning, is implemented by the change of synaptic weight. The typical behaviour of potentiation and depression corresponds to the positive and negative change of synaptic weight, which can be modified through consecutive spikes [47]. By applying five consecutive positive voltages (0–1 V) and negative voltages (0 to −2 V), the current incrementally increased and decreased respectively, as shown in Fig. 5(a, b). Based on the incremental change of the device conductance, the current was served as synaptic weight to emulate the synaptic behaviours (Fig. 5(c)). When a series of positive pulses (+1 V) are applied, the current is gradually increased and the device is potentiated. On the contrary, depression occurs after subsequent application of negative pulses (−1 V). In addition, 2×10^4 pulse cycles were successfully applied and no noticeable degradation was observed, indicating a great device performance (Fig. 6(a–c)). The STDP as a fundamental learning rule for the emulation of synaptic functions is demonstrated as well based on the precise timing between pre- and post-synaptic spikes. We applied a pair of square pulses with amplitude V^+/V^- = 1 V/−1 V, pulse width 10 ms and pulse period 20 ms between the top and bottom electrode which acted as the pre- and post-synaptic spikes. The relative spiking timing Δt was defined as the time interval between the launch of each paired spikes. The current levels were measured before (I_1) and after (I_2) the application of pre- and post-spike pairs. The change in synaptic weight (Δw) was described as $(I_2 - I_1)/ I_1$. If the pre-spike arrives before the post-synaptic spike ($\Delta t > 0$), synaptic weight increases and a long-term potentiation (LTP) occurs. On the contrary, if the post-synaptic spike is triggered after the pre-spike ($\Delta t < 0$), synaptic weight decreases and a long-term depression (LTD) is achieved. In addition, the change of synaptic weight becomes smaller at bigger Δt, as shown in Fig. 6(d) [17,48]. Based on the aforementioned results, it is concluded that the RGO layer plays a significant role in the reported switching performance. Specifically, the observed nonlinearity is originated from the $SrTiO_3$/RGO interface modification as the RGO is more conductive than the interface, which was consistent with the previous study [49].

We found that Ag filaments can be easily formed in the $SrTiO_3$ nanoparticles film but not in RGO layer due to the low diffusion rate of silver through the RGO layer. Otherwise, an abrupt change of resistance will be found and also I_{cc} is required to tune conductance state. The resistances of LRS in both devices are comparable because I_{cc} was applied to the device without RGO in order to avoid excessive Ag diffusion. Nevertheless, the resistance of HRS in Ag/$SrTiO_3$/FTO was higher than that in Ag/$SrTiO_3$/RGO/FTO. When the former device was in LRS, Ag filaments that exhibited higher thermal conductivity than $SrTiO_3$ are created with regions of high temperature distributed around them. Upon application of a negative voltage, random rupture of conductive filaments occurred due to the uniform Joule heating. The Ag/$SrTiO_3$/RGO/FTO device presents a very different behaviour. The LRS is also obtained when filaments reached the RGO; however, because of the high interfacial resistance, most of the voltage is applied to the interface and the

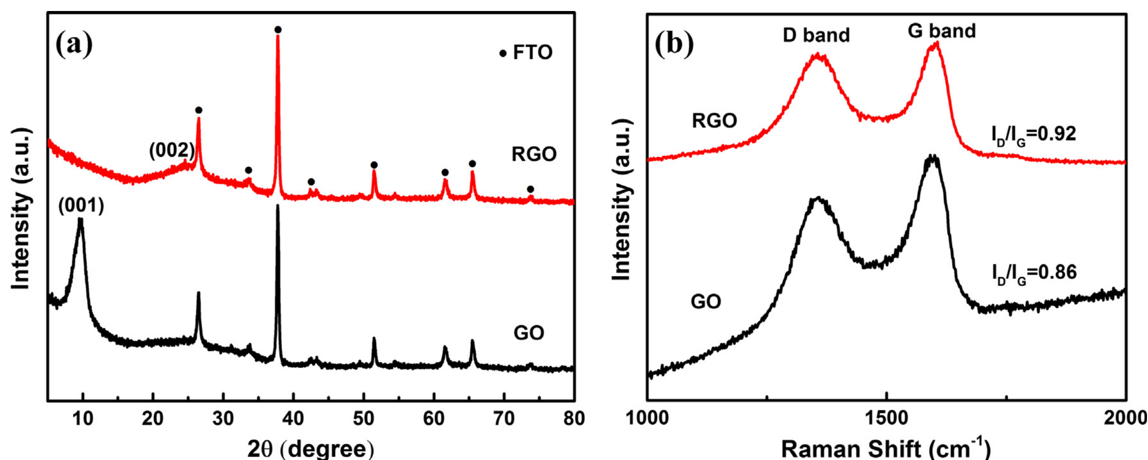

Fig. 3. (a) XRD patterns and (b) Raman spectra of GO and RGO.

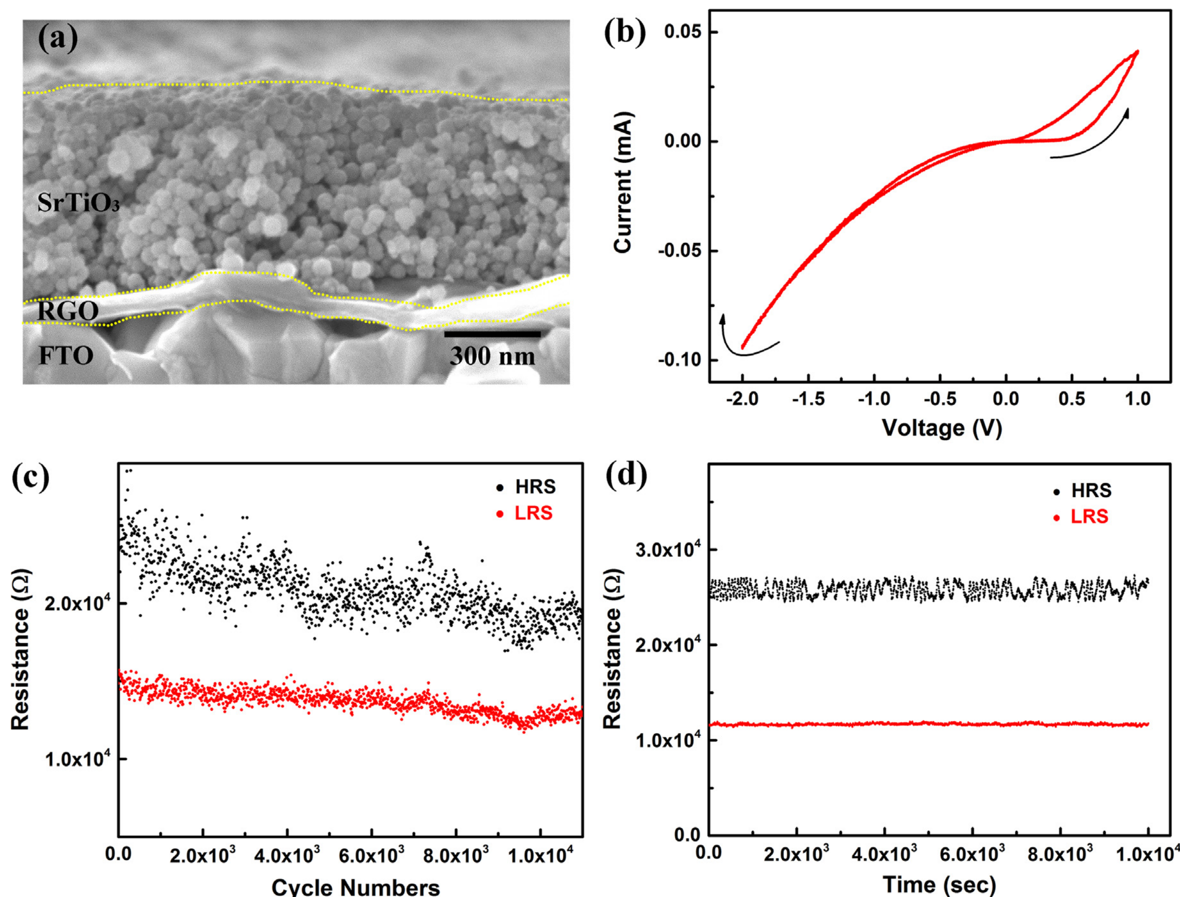

Fig. 4. (a) The cross-sectional SEM image of $SrTiO_3$/RGO/FTO. (b) I-V curve of Ag/$SrTiO_3$/RGO/FTO. The arrows represent the sweep direction. (c) Endurance test of the device. Set and reset pulses are +1 V and −1 V respectively with duration of 10 ms. (d) Retention test of the device at room temperature.

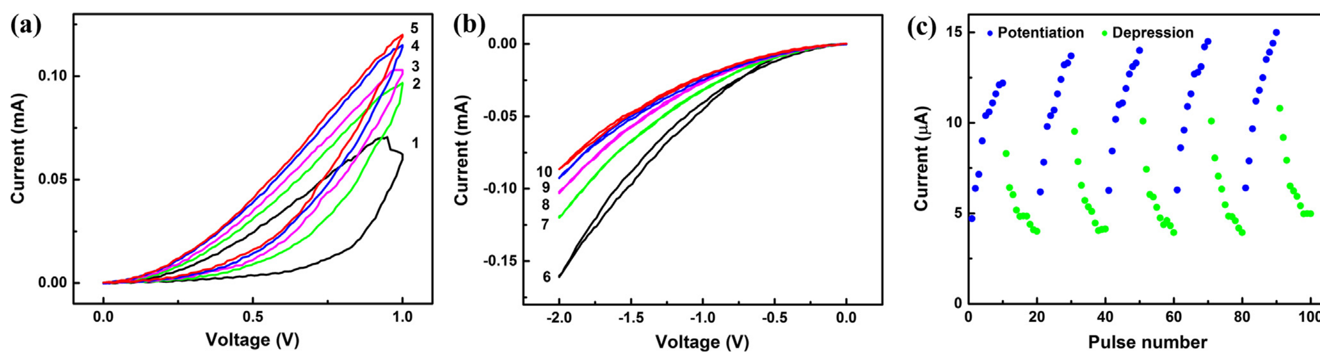

Fig. 5. I-V curves of Ag/$SrTiO_3$/RGO/FTO under five consecutive (a) positive and (b) negative voltage sweeps. (c) Pulse response of the device with +1 V for potentiation and −1 V for depression.

generated Joule heat is dissipated through the RGO. Hence, the random rupture of filaments is unlikely, similar to the result reported in a polymer device [30]. Instead, the filaments are directly disconnected from the graphene layer, thereby leading to the reset process, as previously reported. Accordingly, the low density of state (DOS) near the Dirac points and tunneling probability between the remaining filament and RGO contributed to HRS [31].

However, in this study, the area of switching loop in the negative region is small and no obvious reset process is observed, which differs from some previous studies. It indicates that the filaments in this work were not disconnected from RGO. This is attributed to the porous structure of the nanoparticles film, which was beneficial for the excessive injection of Ag^+, beyond the requirement of filaments formation. Thus, strong filaments are created, whereas controlled growth of filaments can be realized by varying I_{cc} in device without RGO. Furthermore, the presence of RGO layer with high thermal conductivity and large area make the strong filaments more difficult to rupture under applied negative voltage. Correspondingly, the gradual dissolution of filaments at the interface is expected, resulting in the analog switching with a small on/off ratio. It can be speculated that the modulation of filament morphology is responsible for the switching behaviour in RGO sample rather than the modulation of the tunnel barrier length. Graphene is well known to show metallic conductivity in plane, but exhibits high out-of-plane resistance from two contacting graphene flakes. By varying the overlap area between graphene flakes, different

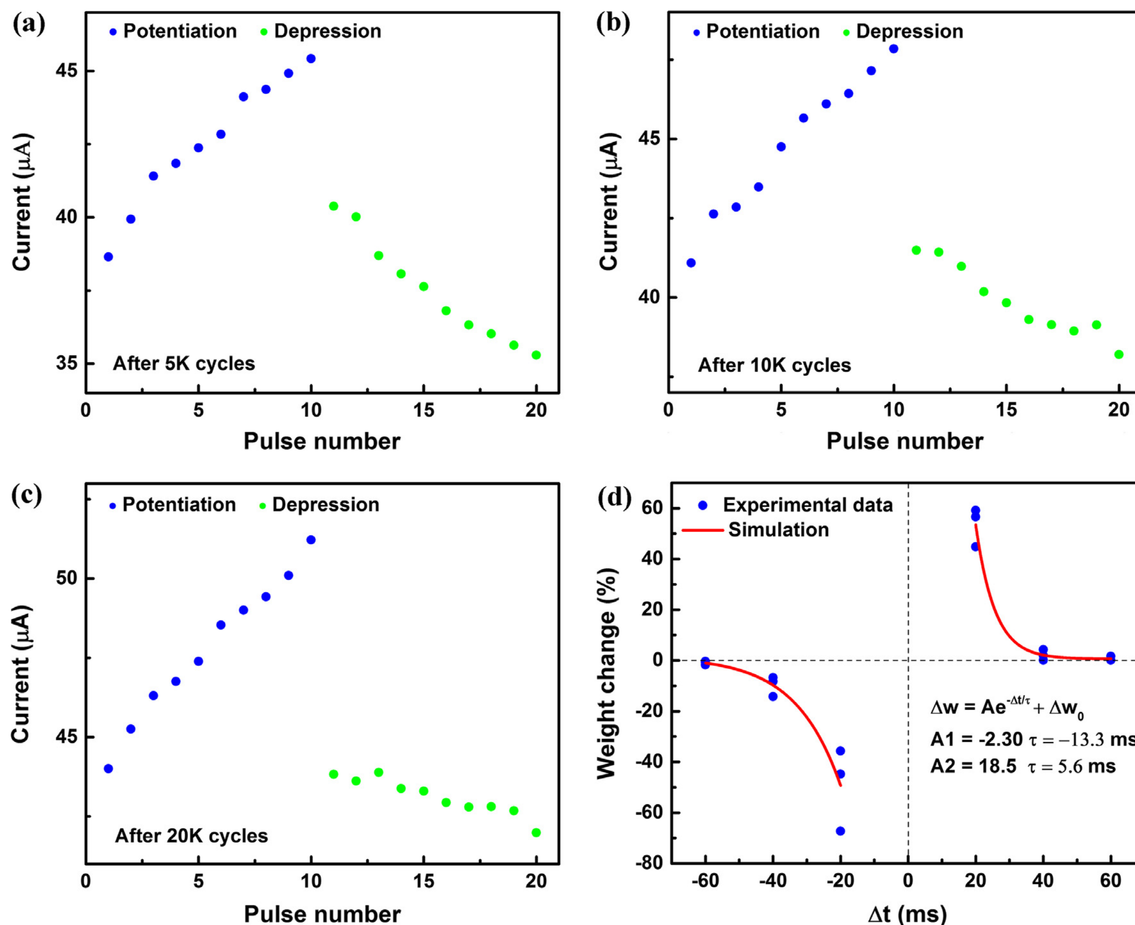

Fig. 6. Endurance test of Ag/$SrTiO_3$/RGO/FTO under consecutive potentiation (+1 V, 10 ms) and depression (−1 V, 10 ms). (a) After 5 K cycles; (b) after 10 K cycles; (c) after 20 K cycles. (d) The synaptic weight change versus the relative spike timing (Δt). The solid lines are the exponential fits to the data.

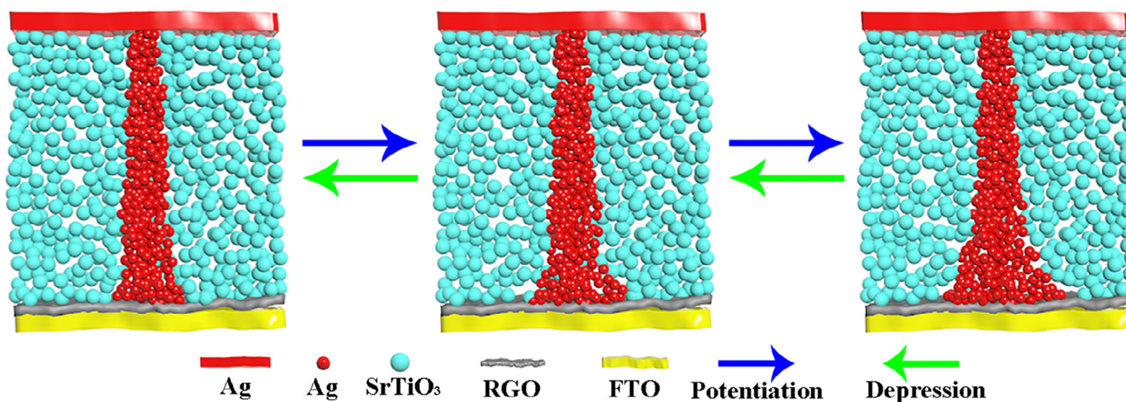

Fig. 7. Schematic illustration of potentiation and depression behaviours under consecutive potentiation and depression pulses.

number of conductive pathway is provided, which results in controlled resistance [50,51]. This is also the case for the formed Ag filaments that exhibit different overlap areas with RGO. Specifically, when the overlap areas are increased, decreased resistance can be expected under repeated positive pulses, and vice versa under negative voltages (Fig. 7). Consequently, the potentiation and depression behaviours are realized by the rearrangement of the filament's atomic structure and tunable interfacial resistance with repeated pulses.

4. Conclusions

In conclusion, resistive switching performances of $SrTiO_3$ nanoparticles based films fabricated by facile solution-based method, were investigated. The digital switching behaviour found in the device using Ag as the top electrode was attributed to formation/rupture of Ag filaments. Additionally, the growth of filaments was further controlled by applying different I_{cc}. After inserting the reduced graphene oxide layer, an analog switching behaviour was

observed, and typical potentiation and depression behaviours were achieved as well. For the reduced graphene oxide, it showed lower resistance than the interface and can act as a barrier for the Ag penetration. Moreover, the large reduced graphene oxide layer with high thermal conductivity was beneficial for the Joule heating dissipation. As a result, strong Ag filaments in $SrTiO_3$ can hardly be broken under negative voltage, but can be tuned by repeated positive or negative cycles. The obtained different overlap areas between filaments and reduced graphene oxide contributed to the modulation of the interfacial resistance and the nonlinear I-V characteristics.

Acknowledgements

This work was supported by the Australian Research Council Project of FT140100032.

References

[1] Z. Wang, L. Wang, M. Nagai, L. Xie, M. Yi, W. Huang, Nanoionics-enabled memristive devices: strategies and materials for neuromorphic applications, Adv. Electron. Mater. 3 (2017) 1600510.
[2] J.J. Yang, D.B. Strukov, D.R. Stewart, Memristive devices for computing, Nat Nanotechnol. 8 (1) (2013) 13–24.
[3] Y. Jeong, S. Kim, W.D. Lu, Utilizing multiple state variables to improve the dynamic range of analog switching in a memristor, Appl. Phys. Lett. 107 (17) (2015) 173105.
[4] K. Qian, R.Y. Tay, M.-F. Lin, J. Chen, H. Li, J. Lin, J. Wang, G. Cai, V.C. Nguyen, E.H. T. Teo, T. Chen, P.S. Lee, Direct observation of indium conductive filaments in transparent flexible, and transferable resistive switching memory, ACS Nano 11 (2017) 1712–1718.
[5] B.K. You, W.I. Park, J.M. Kim, K.-I. Park, H.K. Seo, J.Y. Lee, Y.S. Jung, K.J. Lee, Reliable control of filament formation in resistive memories by self-assembled nanoinsulators derived from a block copolymer, ACS Nano 8 (9) (2014) 9492–9502.
[6] S.K. Kim, J.Y. Kim, B.C. Jang, M.S. Cho, S.Y. Choi, J.Y. Lee, H.Y. Jeong, Conductive graphitic channel in graphene oxide-based memristive devices, Adv. Funct. Mater. 26 (41) (2016) 7406–7414.
[7] Q. Liu, J. Sun, H. Lv, S. Long, K. Yin, N. Wan, Y. Li, L. Sun, M. Liu, Real-time observation on dynamic growth/dissolution of conductive filaments in oxide-electrolyte-based ReRAM, Adv. Mater. 24 (14) (2012) 1844–1849.
[8] G.-S. Park, Y.B. Kim, S.Y. Park, X.S. Li, S. Heo, M.-J. Lee, M. Chang, J.H. Kwon, M. Kim, U.-I. Chung, In situ observation of filamentary conducting channels in an asymmetric Ta_2O_{5-x}/TaO_{2-x} bilayer structure, Nat. Commun. 4 (2013).
[9] C.F. Chang, J.Y. Chen, C.W. Huang, C.H. Chiu, T.Y. Lin, P.H. Yeh, W.W. Wu, Direct observation of dual-filament switching behaviors in Ta_2O_5-based memristors, Small 13 (2017) 1603116.
[10] H. Tian, H.-Y. Chen, B. Gao, S. Yu, J. Liang, Y. Yang, D. Xie, J. Kang, T.-L. Ren, Y. Zhang, Monitoring oxygen movement by Raman spectroscopy of resistive random access memory with a graphene-inserted electrode, Nano Lett. 13 (2) (2013) 651–657.
[11] F. Fan, B. Zhang, Y. Cao, Y. Chen, Solution-processable poly (N-vinylcarbazole)-covalently grafted MoS_2 nanosheets for nonvolatile rewritable memory devices, Nanoscale 9 (7) (2017) 2449–2456.
[12] Y. Wang, Q. Liu, S. Long, W. Wang, Q. Wang, M. Zhang, S. Zhang, Y. Li, Q. Zuo, J. Yang, Investigation of resistive switching in Cu-doped HfO_2 thin film for multilevel non-volatile memory applications, Nanotechnology 21 (4) (2009) 045202.
[13] H. Wang, F. Meng, Y. Cai, L. Zheng, Y. Li, Y. Liu, Y. Jiang, X. Wang, X. Chen, Sericin for resistance switching device with multilevel nonvolatile memory, Adv. Mater. 25 (38) (2013) 5498–5503.
[14] H.-S. PhilipáWong, Multi-level control of conductive nano-filament evolution in HfO_2 ReRAM by pulse-train operations, Nanoscale 6 (11) (2014) 5698–5702.
[15] J.H. Yoon, K.M. Kim, S.J. Song, J.Y. Seok, K.J. Yoon, D.E. Kwon, T.H. Park, Y.J. Kwon, X. Shao, C.S. Hwang, $Pt/Ta_2O_5/HfO_{2-x}/Ti$ resistive switching memory competing with multilevel NAND flash, Adv. Mater. 27 (25) (2015) 3811–3816.
[16] J.-D. Kim, Y.-J. Baek, Y. Jin Choi, C. Jung Kang, H. Ho Lee, H.-M. Kim, K.-B. Kim, T.-S. Yoon, Investigation of analog memristive switching of iron oxide nanoparticle assembly between Pt electrodes, J. Appl. Phys. 114 (22) (2013) 224505.
[17] Z.Q. Wang, H.Y. Xu, X.H. Li, H. Yu, Y.C. Liu, X.J. Zhu, Synaptic learning and memory functions achieved using oxygen ion migration/diffusion in an amorphous InGaZnO memristor, Adv. Funct. Mater. 22 (13) (2012) 2759–2765.
[18] E. Yoo, M. Lyu, J.-H. Yun, C. Kang, Y. Choi, L. Wang, Bifunctional resistive switching behavior in an organolead halide perovskite based $Ag/CH_3NH_3PbI_{3-x}Cl_x/FTO$ structure, J. Mater. Chem. C 4 (33) (2016) 7824–7830.
[19] T. Shi, R. Yang, X. Guo, Coexistence of analog and digital resistive switching in $BiFeO_3$-based memristive devices, Solid State Ionics 296 (2016) 114–119.
[20] C.-S. Yang, D.-S. Shang, Y.-S. Chai, L.-Q. Yan, B.-G. Shen, Y. Sun, Moisture effects on the electrochemical reaction and resistance switching at Ag/molybdenum oxide interfaces, Phys. Chem. Chem. Phys. 18 (18) (2016) 12466–12475.
[21] X. Li, H. Wu, B. Gao, W. Wu, D. Wu, N. Deng, J. Cai, H. Qian, Electrode-induced digital-to-analog resistive switching in TaO_x-based RRAM devices, Nanotechnology 27 (30) (2016) 305201.
[22] H.J. Kim, Y.-J. Baek, Y.J. Choi, C.J. Kang, H.H. Lee, H.-M. Kim, K.-B. Kim, T.-S. Yoon, Digital versus analog resistive switching depending on the thickness of nickel oxide nanoparticle assembly, RSC Adv. 3 (43) (2013) 20978–20983.
[23] Y.-S. Chen, P.-S. Chen, H.-Y. Lee, T.-Y. Wu, K.-H. Tsai, F. Chen, M.-J. Tsai, Enhanced endurance reliability and low current operation for AlO_x/HfO_x based unipolar RRAM with Ni electrode, Solid State Electron. 94 (2014) 1–5.
[24] S. Rahaman, S. Maikap, W. Chen, H. Lee, F. Chen, T. Tien, M. Tsai, Impact of TaO_x nanolayer at the $GeSe_x/W$ interface on resistive switching memory performance and investigation of Cu nanofilament, J. Appl. Phys. 111 (6) (2012) 063710.
[25] X.Y. Li, X.L. Shao, Y.C. Wang, H. Jiang, C.S. Hwang, J.S. Zhao, Thin TiO_x layer as a voltage divider layer located at the quasi-Ohmic junction in the $Pt/Ta_2O_5/Ta$ resistance switching memory, Nanoscale 9 (6) (2017) 2358–2368.
[26] X. Zhao, S. Liu, J. Niu, L. Liao, Q. Liu, X. Xiao, H. Lv, S. Long, W. Banerjee, W. Li, S. Si, M. Liu, Confining cation injection to enhance CBRAM performance by nanopore graphene layer, Small 13 (2017) 1603948.
[27] S. Liu, N. Lu, X. Zhao, H. Xu, W. Banerjee, H. Lv, S. Long, Q. Li, Q. Liu, M. Liu, Eliminating negative-SET behavior by suppressing nanofilament overgrowth in cation-based memory, Adv. Mater. 28 (48) (2016) 10623–10629.
[28] J.H. Bong, S.J. Yoon, A. Yoon, W.S. Hwang, B.J. Cho, Ultrathin graphene and graphene oxide layers as a diffusion barrier for advanced Cu metallization, Appl. Phys. Lett. 106 (6) (2015) 063112.
[29] J. Hong, S. Lee, S. Lee, H. Han, C. Mahata, H.-W. Yeon, B. Koo, S.-I. Kim, T. Nam, K. Byun, Graphene as an atomically thin barrier to Cu diffusion into Si, Nanoscale 6 (13) (2014) 7503–7511.
[30] B.C. Jang, H. Seong, J.Y. Kim, B.J. Koo, S.K. Kim, S.Y. Yang, S.G. Im, S.-Y. Choi, Ultra-low power, highly uniform polymer memory by inserted multilayer graphene electrode, 2D Mater. 2 (4) (2015) 044013.
[31] M. Qian, Y. Pan, F. Liu, M. Wang, H. Shen, D. He, B. Wang, Y. Shi, F. Miao, X. Wang, Tunable, ultralow-power switching in memristive devices enabled by a heterogeneous graphene-oxide interface, Adv. Mater. 26 (20) (2014) 3275–3281.
[32] T. Wan, B. Qu, H. Du, X. Lin, P. Guan, Q. Lin, N. Chen, T.T. Tan, T. Hang, D. Chu, Tunable resistance switching in solution processed chromium-doped strontium titanate nanoparticles films, J. Colloid Interface Sci. 494 (2017) 178–184.
[33] K.H. Choi, J. Ali, Y.H. Doh, Exploring resistive switching in poly (4-vinylphenol)–graphene nano-composite films, Jpn. J. Appl. Phys. 54 (3) (2015) 035103.
[34] C. Zhu, S. Zhu, K. Zhang, Z. Hui, H. Pan, Z. Chen, Y. Li, D. Zhang, D.-W. Wang, Confined SnO_2 quantum-dot clusters in graphene sheets as high-performance anodes for lithium-ion batteries, Sci. Rep. 6 (2016) 25829.
[35] H.-S. Jang, J.-M. Yun, D.-Y. Kim, D.-W. Park, S.-I. Na, S.-S. Kim, Moderately reduced graphene oxide as transparent counter electrodes for dye-sensitized solar cells, Electrochim. Acta 81 (2012) 301–307.
[36] F. Zhuge, B. Hu, C. He, X. Zhou, Z. Liu, R.-W. Li, Mechanism of nonvolatile resistive switching in graphene oxide thin films, Carbon 49 (12) (2011) 3796–3802.
[37] Y. Li, S. Long, M. Zhang, Q. Liu, L. Shao, S. Zhang, Y. Wang, Q. Zuo, S. Liu, M. Liu, Resistive switching properties of $Au/ZrO_2/Ag$ structure for low-voltage nonvoltaile memory applications, IEEE Electron Device Lett. 31 (2) (2010) 117–119.
[38] S. La Barbera, D. Vuillaume, F. Alibart, Filamentary switching: synaptic plasticity through device volatility, ACS Nano 9 (1) (2015) 941–949.
[39] W.A. Hubbard, A. Kerelsky, G. Jasmin, E. White, J. Lodico, M. Mecklenburg, B. Regan, Nanofilament formation and regeneration during Cu/Al_2O_3 resistive memory switching, Nano Lett. 15 (6) (2015) 3983–3987.
[40] S.J. Choi, G.S. Park, K.H. Kim, S. Cho, W.Y. Yang, X.S. Li, J.H. Moon, K.J. Lee, K. Kim, In situ observation of voltage-induced multilevel resistive switching in solid electrolyte memory, Adv. Mater. 23 (29) (2011) 3272–3277.
[41] U. Celano, L. Goux, A. Belmonte, K. Opsomer, R. Degraeve, C. Detavernier, M. Jurczak, W. Vandervorst, Understanding the dual nature of the filament dissolution in conductive bridging devices, J. Phys. Chem. Lett. 6 (10) (2015) 1919–1924.
[42] H. Lv, X. Xu, H. Liu, R. Liu, Q. Liu, W. Banerjee, H. Sun, S. Long, L. Li, M. Liu, Evolution of conductive filament and its impact on reliability issues in oxide-electrolyte based resistive random access memory, Sci. Rep. 5 (2015) 7764.
[43] A.M. Rana, T. Akbar, M. Ismail, E. Ahmad, F. Hussain, I. Talib, M. Imran, K. Mehmood, K. Iqbal, M.Y. Nadeem, Endurance and cycle-to-cycle uniformity improvement in tri-layered $CeO_2/Ti/CeO_2$ resistive switching devices by changing top electrode material, Sci. Rep. 7 (2017) 39539.
[44] S. Some, P. Bhunia, E. Hwang, K. Lee, Y. Yoon, S. Seo, H. Lee, Can commonly used hydrazine produce n-type graphene?, Chem Eur. J. 18 (25) (2012) 7665–7670.
[45] L. Qiu, H. Zhang, W. Wang, Y. Chen, R. Wang, Effects of hydrazine hydrate treatment on the performance of reduced graphene oxide film as counter electrode in dye-sensitized solar cells, Appl. Surf. Sci. 319 (2014) 339–343.
[46] N. Wu, X. She, D. Yang, X. Wu, F. Su, Y. Chen, Synthesis of network reduced graphene oxide in polystyrene matrix by a two-step reduction method for superior conductivity of the composite, J. Mater. Chem. 22 (33) (2012) 17254–17261.

[47] D.S. Jeong, I. Kim, M. Ziegler, H. Kohlstedt, Towards artificial neurons and synapses: a materials point of view, RSC Adv. 3 (10) (2013) 3169–3183.
[48] C. Du, W. Ma, T. Chang, P. Sheridan, W.D. Lu, Biorealistic implementation of synaptic functions with oxide memristors through internal ionic dynamics, Adv. Funct. Mater. 25 (27) (2015) 4290–4299.
[49] M. Wang, X. Lian, Y. Pan, J. Zeng, C. Wang, E. Liu, B. Wang, J.J. Yang, F. Miao, D. Xing, A selector device based on graphene–oxide heterostructures for memristor crossbar applications, Appl. Phys. A 120 (2) (2015) 403–407.
[50] M. Hempel, D. Nezich, J. Kong, M. Hofmann, A novel class of strain gauges based on layered percolative films of 2D materials, Nano Lett. 12 (11) (2012) 5714–5718.
[51] Z. Chen, T. Ming, M.M. Goulamaly, H. Yao, D. Nezich, M. Hempel, M. Hofmann, J. Kong, Enhancing the sensitivity of percolative graphene films for flexible and transparent pressure sensor arrays, Adv. Funct. Mater. 26 (28) (2016) 5061–5067.